

3D FEM MODELING AND TECHNOLOGY OF PIEZO-ELECTRIC RING MEMS ANTENNA

A. Massaro^{1,*}, R. Cingolani¹, and A. Passaseo²

¹IIT Italian Institute of Technology, Center of Bio-Molecular Nanotechnology, Arnesano 73100, Italy

²National Nanotechnology Laboratory, Institute of Nanoscience of CNR, Lecce 73100, Italy

Abstract—Actually MEMS technology allows to fabricate free standing and bended cantilevers by acting on stress/strain properties and thicknesses of materials. In particular, by means of MEMS technology it is possible to realize ring or spiral layouts with piezoelectric materials. The mechanical movement due to the piezoelectric resonance can be used in order to modulate a signal travelling in the MEMS and radiating in the free space as happens in antennas. In this work we provide an accurate study regarding the design approach of piezoelectric aluminium nitride (AlN) ring antenna. The study is developed by means of a tailored 3D FEM tool which allows to analyze the piezoelectric resonances and to design the ring micro-antenna in the THz range. Finally we provide the technology and we measure the piezoelectric resonances of ring antennas.

1. INTRODUCTION

Research in the field of MEMS resonator has generated different techniques using electrically coupled resonators especially for realizing bandpass filters [1–6]. Particular geometries, such as ring layouts, are preferred for their strong resonance due to the ring/cavity resonance. In particular, by combining the ring cavity effect with the high AlN piezoelectric resonance it is possible to achieve MEMS filters [1–3] or micro-antennas [7–12] with high performances. Achieving properly dimensions the piezoelectric ring matches with a GHz/THz signal which can be coupled with the ring (open loop) and radiated in the

Received 30 June 2011, Accepted 23 July 2011, Scheduled 9 August 2011

* Corresponding author: Alessandro Massaro (alessandro.massaro@iit.it).

space surrounding the structure. According with the dimensions, the proposed structure will behave as a dipole/small dipole [13] for RF/THz wireless applications. The piezoelectric frequencies resonance may change the ring diameter and in general the geometrical configuration as indicated in Fig. 1 where is reported the scheme of a transmitter/receiver radiation system and some kinds of ring deformations. The geometrical deformation of the transmitter ring can modulates the phase or the amplitude (variation of the radiation resistance due to the geometrical deformation [14]) of a transmitted GHz/THz signal: the modulation is due to the piezoelectric effect of the AlN piezoelectric layer and is performed by applying a resonance control signal which can be found at lower frequencies. The proposed paper is developed as follows: (i) we first analyze by means of a three dimensional (3D) finite element method (FEM) approach the piezoelectric resonance effect of an AlN ring MEMS; (ii) we design (3D FEM) a AlN micro-antenna in the THz range; (iii) then we provide the technological aspects in order to fabricate Molybdenum/AluminiumNitride/Molybdenum (Mo/AlN/Mo) ring or helical MEMS antenna; (iv) finally we measure the piezoelectric resonances of a ring antenna.

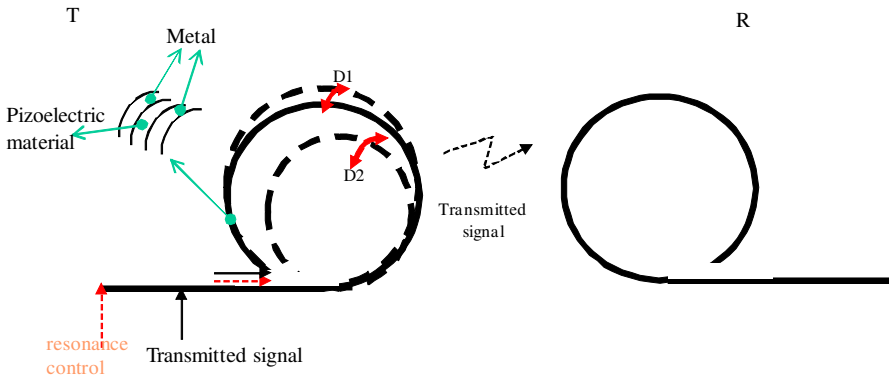


Figure 1. Schematic principle of radiation application between a transmitter T and a receiver R piezoelectric ring antennas. The transmitter antenna T is characterized by a transmitted signal which can be modulated through the piezoelectric effect (piezoelectric resonance due to the resonance control signal). The deformations D_1 and D_2 are related to the piezoelectric resonance frequency.

2. FEM MODELING AND THEORETICAL ASPECTS OF RING MEMS ANTENNAS

In order to study the piezoelectric resonance which will provide the motion of the transmitter ring MEMS (RMEMS), and, consecutively, the phase/amplitude modulation of the transmitted signal, we model the structure by means of a 3D FEM properly designed tool. The used FEM tool analyzes this piezoelectric effect of the AlN layer through the stress relationships between the stress \mathbf{T} , the strain \mathbf{S} , electric field \mathbf{E} , and electric displacement field \mathbf{D}

$$\begin{aligned}\mathbf{T} &= c_E \mathbf{S} - e^T \mathbf{D} \\ \mathbf{D} &= e \mathbf{S} - \varepsilon_r \mathbf{E}\end{aligned}\quad (1)$$

where c_E , e , and ε_r are the elasticity matrix, the coupling matrix and the relative permittivity matrix, respectively, defined for the AlN material as (FEMLAB libraries)

$$c_E = \begin{pmatrix} 4.1e^{11} & 1.49e^{11} & 9.9e^{10} & 0 & 0 & 0 \\ 1.49e^{11} & 4.1e^{11} & 1.49e^{11} & 0 & 0 & 0 \\ 9.9e^{10} & 1.49e^{11} & 3.89e^{11} & 0 & 0 & 0 \\ 0 & 0 & 0 & 1.25e^{11} & 0 & 0 \\ 0 & 0 & 0 & 0 & 1.25e^{11} & 0 \\ 0 & 0 & 0 & 0 & 0 & 1.25e^{11} \end{pmatrix} [\text{Pa}] \quad (2)$$

$$e = \begin{pmatrix} 0 & 0 & 0 & 0 & -0.48 & 0 \\ 0 & 0 & 0 & -0.48 & 0 & 0 \\ -0.58 & -0.58 & 1.55 & 0 & 0 & 0 \end{pmatrix} [\text{C} / \text{m}^2] \quad (3)$$

$$\varepsilon_r = \begin{pmatrix} 9 & 0 & 0 \\ 0 & 9 & 0 \\ 0 & 0 & 9 \end{pmatrix} \quad (4)$$

The deformation d of the structure is calculated by

$$d = \sqrt{\sum_i u_i^2} \quad (5)$$

where u_i represents the spatial displacement along the x ($i = 1$), y ($i = 2$), and z ($i = 3$) directions. By implementing the model we obtain for an AlN ring MEMS with a diameter of 410 μm and a width of 41 μm the piezoelectric resonances reported in Fig. 2 and Fig. 3. The calculated piezoelectric resonance frequencies will define the resonance control signal. These frequencies will change with the geometrical dimensions and shape of the MEMS. The 3D FEM modal deformation for both resonant modes of Figs. 2 and 3 are calculated by applying a voltage signal between the two metals electrodes reported in the layout

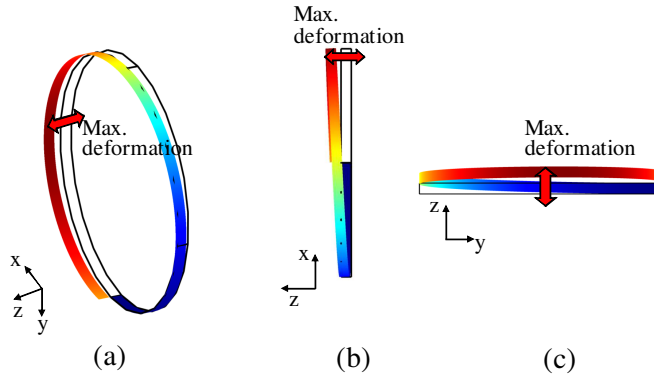


Figure 2. Maximum piezoelectric deformation of the ring MEMS by applying a resonance control signal of 343 Hz (resonance frequency). The deformation is calculated (a) in the 3D space, (b) in $(x-z)$ perspective, and (c) in the $(z-y)$ perspective.

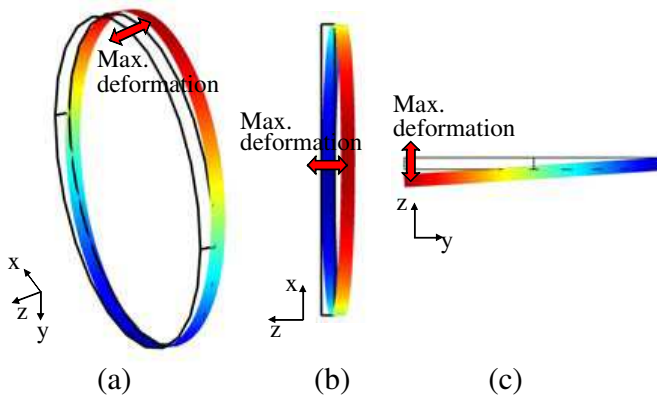


Figure 3. Maximum piezoelectric deformation of the ring MEMS by applying a resonance control signal of 128 Hz (resonance frequency). The deformation is calculated (a) in the 3D space, (b) in $(x-z)$ perspective, and (c) in the $(z-y)$ perspective.

scheme of Fig. 1: a FEM deformation of the order of ten microns is observed by applying 10 V to the electrodes. Concerning the radiation aspects, we observe that, according with theory [13], a wire antenna whose lengths are usually $\lambda/50 < l \leq \lambda/10$ behaves as infinitesimal dipole (small dipole). For this purpose, considering diameters between 100 to 800 μm and lengths between 250 μm and 3 mm, the proposed structure will behaves as a small dipole or a dipole working from GHz to

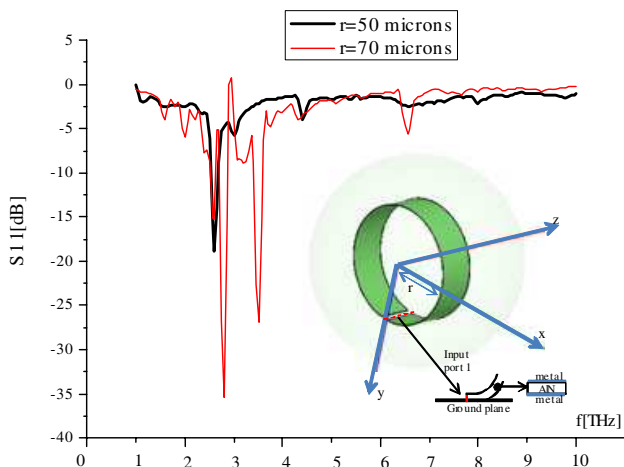


Figure 4. Scattering parameter S_{11} evaluated at the input port. Inset: 3D FEM modeling of the ring receiver antenna.

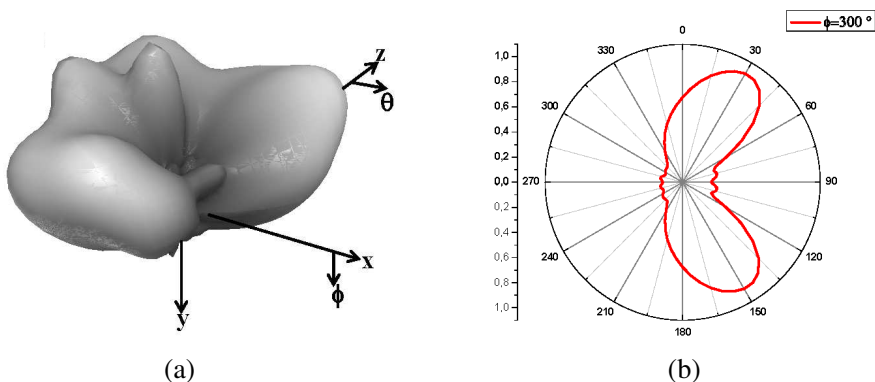


Figure 5. (a) 3D far field radiation pattern of the total electric field. (b) Total field versus θ or $\phi = 300$ deg.

THz. In order to design a micro-antenna we analyze the key scattering parameter at the input port of the ring structure (S_{11} parameter) which defines the reflectivity at the input port (see inset of Fig. 4). A low reflectivity will indicate a good matching with a source and a high transferred power. Focusing on ring diameters of $100 \mu\text{m}$ and $140 \mu\text{m}$ we find good performances at working frequencies between 2.6 THz and 3.6 THz (see the S_{11} parameter reported in Fig. 4). By fixing the working frequency at 2.6 THz for the ring with radius $r = 50 \mu\text{m}$, the antenna will be characterized by the 3D radiation pattern of Fig. 5(a)

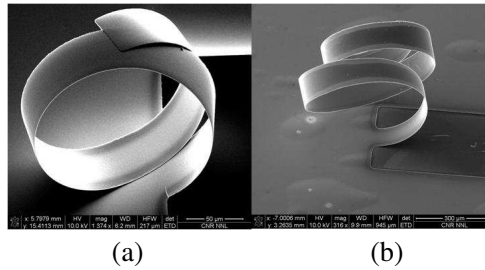


Figure 7. SEM images of the Mo/AlN/Mo ring/helical MEMS.

high residual stress of the films. Rings of different geometries (40–50 μm -wide and 1000, 1500, 2000 and 2500 μm -long) were fabricated using conventional micromachining techniques involving the sacrificial oxide layer etching to release the microstructures forming rings. The rings come out from strips of an AlN thin piezoelectric layer between two Molybdenum metallic electrodes. Different steps of optical lithography and well-controlled both dry and wet etching are used to define the pattern of ring. A step of lithography and wet chemical etching H_2O_2 based solution is used to define windows to expose Mo bottom electrodes, while the top electrode consists of the upper Mo layer. After the fabrication of electrodes a further lithographic patterning followed by dry and wet etching is necessary to define the windows where the surface of the sacrificial layer is exposed. A SiCl_4 based plasma by Inductively Coupled Plasma (ICP) dry etching using a photoresist mask is used to remove the upper Molybdenum layer and the AlN layer, while the lower Molybdenum layer is etched by a H_2O_2 based solution. Finally a HF-based solution is used to remove the SiO_2 sacrificial layer allowing the release of the rings from the substrate surface. The high residual stress of the layered structure brings to the rolling up of the realized strips forming the rings. A properly combination of layer thicknesses and conditions of deposition will define the ring diameter and configuration: example of ring and helical layouts are reported in Fig. 7(a) and Fig. 7(b), respectively.

4. CONTROL OF THE FABRICATION PROCESS

The Mo layer 1 and the AlN layer of Fig. 6 provide a high residual stress improving a radius of curvature of the layered structure. By “tuning” the Mo layer 1 thickness it is possible to control the curvature of the ring for a fixed total length L , width w (see L and w parameter reported in Fig. 8). The tuning process is performed by acting on the Mo deposition time of the RF sputtering machine working on fixed

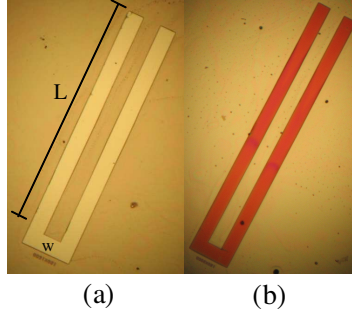


Figure 8. Definition of the geometrical parameter L . (a) Refers to the step (d) and (b) refers to the step (e) of Fig. 6.

Table 1. Different cases of controlled layouts.

Case	Mo layer 1 thickness [μm]	Length L [μm]	Diameter [μm]	Layout
A	100	250÷500	~ 100	Ring
B	70	250÷500	~ 50	Helical
C	100	500÷750	150÷200	Ring
D	70	500÷750	~ 120	Helical
E	100	750÷1000	400÷500	Ring
F	70	750÷1000	~ 140	Helical

conditions (gas pressures, BIAS, temperature voltage). In order to obtain a controlled process we fix some geometrical parameters such as the Mo layer 2 thickness to 100 nm and the width w to 50 μm and we vary the lengths L from 250 μm to 1000 μm obtaining diameters ranging from 50 μm to 500 μm . All the studied repeatable cases are summarized in the Table 1.

5. EXPERIMENTAL RESULTS OF PIEZOELECTRIC RESONANCES

The piezoelectric characterization of the single ring antenna is experimentally performed by a Karl Suss PA 150, probe station, with tungsten microtips connected with coaxial cables to the Agilent 4980A precision LCR meter. The LCR is controlled by a PC that collects the data. The setup measures the equivalent impedance characteristics, and the equivalent capacitance of the ring antenna.

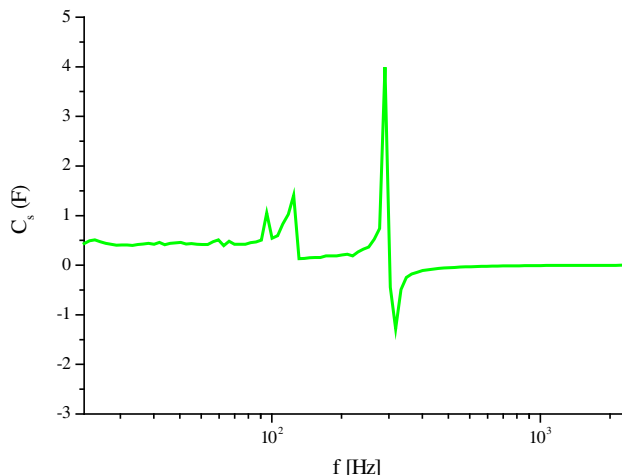


Figure 9. Measured series capacitance C_s of a ring MEMS antenna with a diameter of 140 μm .

The two microtips of the LCR meter, are applied to both the Mo electrodes with a source voltage of 0.3 V, and result in a series $R_s C_s$, where R_s represents the material losses (R_s is of the order of 140 Ω). The experimental piezoelectric resonance of the designed ring antenna is illustrated in Fig. 9 where a piezoelectric resonance is found at 263 Hz. By varying the ring diameter of the MEMS the piezoelectric resonances will change as indicated in Fig. 10 by the experimental characterization at low frequency of a ring MEMS with a radius of 100 μm : below f_2 (found experimentally at 347.6 Hz), the measured capacitance C_s is positive and the measured inductance L_p is negative, whereas, above f_2 the capacitance C_s is negative and the inductance L_p is positive. The first resonance (found experimentally at $f_1 = 120.5$ Hz) is characterized by a discontinuity of the total impedance phase θ ($Z = X e^{j\theta}$), while, at the second resonance f_2 , the phase becomes positive by validating the passage to the inductance behavior. A low error $\Delta f_{1,2} = |f_{1,2} \text{ simulated} - f_{1,2} \text{ measured}|$ of few Hz between the 3D FEM and the experimental resonance frequencies is checked ($\Delta f_1 = 7.5$ Hz and $\Delta f_2 = 4.6$ Hz) in Fig. 11 (see FEM displacement plot), by proving the accurate low frequency characterization. The deformation of the antenna is experimentally estimated by measuring the ring displacement at the piezoelectric resonance by means of a post processing of the image: a deformation of the order between 1 μm and 30 μm , induced by applying a voltage in the range between $\Delta V = 0, 1$ V and $\Delta V = 30$ V is checked in Fig. 10 by proving the possibility to use

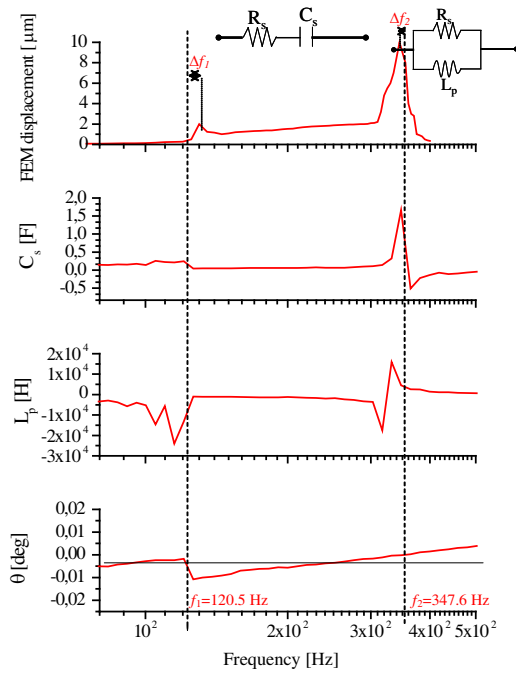


Figure 10. Probe station measurements: circuitual parameters. Capacitance C_s , inductance L_p and impedance phase θ . The measurements are obtained by an input voltage of 0.3 V. The maximum ring displacement is calculated by the 3D FEM approach.

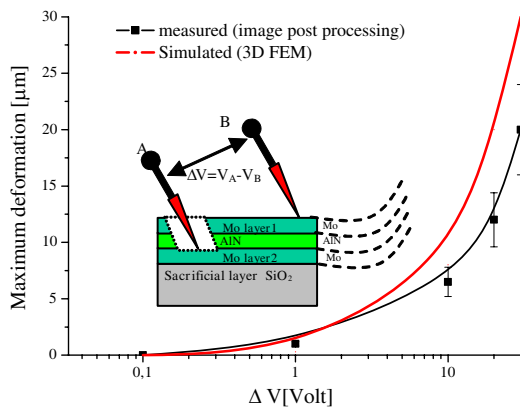


Figure 11. Maximum deformation: comparison between 3D FEM and experimental results. Inset: tips configuration of the LCR meter.

the ring MEMS antenna as a THz modulator as in indicated in scheme of Fig. 1. The principle of amplitude modulation for a transmitter ring is based on the piezoelectric resonance which reduces the ring radius, and, consecutively, the radiated power $P_r = R_r |I_0|^2$, where I_0 is the current travelling the radiation resistance R_r [14].

6. MANUFACTURING ASPECTS

In order to couple different rings on the same chip (see Fig. 12(a)), we have used a mask containing contact layouts. The fabrication of the contact region was performed by considering before the step (a)–(f) of Fig. 6 for the contacts and then the steps (a)–(i) of the same figure for the rings. Fig. 12(b) shows an example of the fabricated contact region where each contact ($50 \mu\text{m} \times 50 \mu\text{m}$) can be contacted by a probe made by three microtips (such as Suss+Microtec probe system): one microtips should contact the Mo layer 2 and the other two microtips should contact the Mo layer 1 as illustrated in Fig. 12(c). Both the kHz signal (signal related to the AlN-resonance) and the THz one (related to the radiation) should be applied on the same Mo conductive layer 1 by means of a configuration reported in the scheme of Fig. 13(a), where the distance D allows to not consider the unwanted interaction between the two signals. Both the kHz/THz signals can be coupled to the ring by the coaxial feeding sources [15] reported in Fig. 13(b). Chemical processes based on lithography and wet chemical

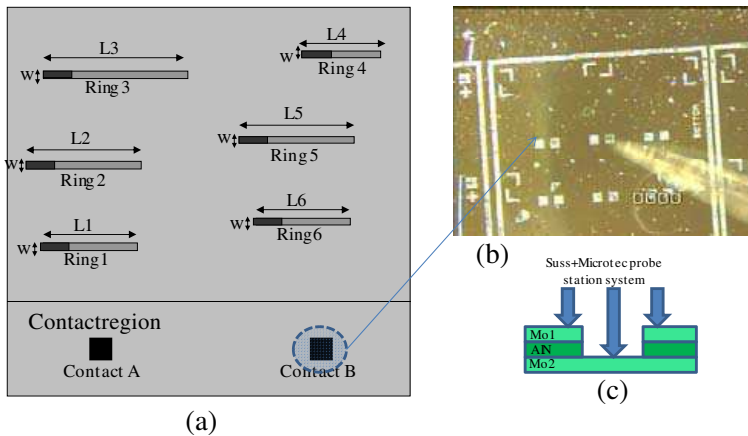


Figure 12. (a) Complete chip containing different ring antennas. (b) Image of a fabricated contact region with different contacts. (c) Cross section of a contact.

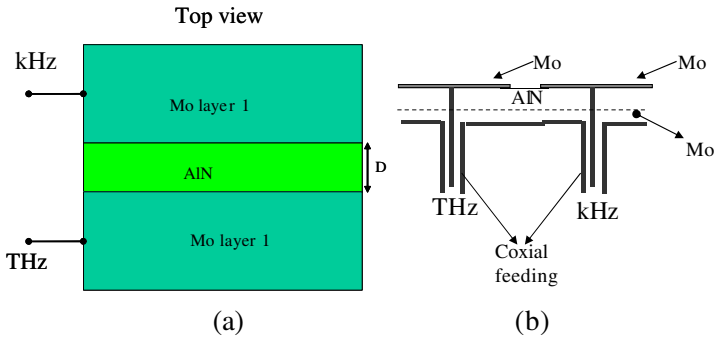


Figure 13. (a) Top view of a possible implementation concerning. (b) cross section of the coaxial feeding configuration.

etching process (processes similar to the case of Fig. 12) can be applied in order to perform the layout of Fig. 13.

7. CONCLUSION

The presented work analyzes the design approach of micro-antennas with ring geometries. The antennas behave as dipole or small dipoles in the RF/THz frequency range and represent a good solution for wireless sensing systems. The simple technology allows to fabricate ring or helical micro-antennas with dimensions used in the design. Experimental piezoelectric characterization about resonances and examples of manufacturing implementations are analyzed. Experimental aspects regarding THz radiation are under investigation.

REFERENCES

1. Piazza, G., P. J. Stephanou, and A. P. Pisano, "Single-chip multiple frequency ALN MEMS filters based on contour-mode piezoelectric resonators," *IEEE J. Microelectromech. Syst.*, Vol. 16, No. 2, 319–328, 2007.
2. Piazza, G., P. J. Stephanou, and A. P. Pisano, "Piezoelectric aluminum nitride vibrating contour mode MEMS resonators," *IEEE J. Microelectromech. Syst.*, Vol. 15, No. 6, 319–328, 2007.
3. Piazza, G., P. J. Stephanou, and A. P. Pisano, "Aluminum Nitride contour-mode vibrating RF MEMS," *IEEE MTT-S Proc. Int. Microw. Symp. Dig.*, 664–667, 2006.

4. Lakin, K. M., "Coupled resonator filters," *Proc. Ultrason. Symp.*, Vol. 1, 901–908, 2002.
5. Cady, W. G., *Piezoelectricity: An Introduction to the Theory and Applications of Electromechanical Phenomena in Crystals*, McGraw-Hill, New York, 1946.
6. Johnson, R. A., *Mechanical Filters in Electronics*, Wiley, New York, 1983.
7. Li, X.-Q., Q.-X. Liu, X.-J. Wu, L. Zhao, J.-Q. Zhang, and Z.-Q. Zhang, "A GW level high-power radial line helical array antenna," *IEEE Trans. Antennas and Propag.*, Vol. 56, No. 9, 2943–2948, 2008.
8. Clark, R. L. and R. N. Dean, "Three dimensional micromachined electromagnetic device and associated methods," US Patent, US 6,271,802 B1, Aug. 7, 2001.
9. Bell, J. M. and M. F. Iskander, "A low-profile Archimedean spiral antenna using an EBG ground plane," *IEEE Trans. Antennas and Propag.*, Vol. 3, 223–226, 2004.
10. Hirose, K., A. Kimizuka, and H. Nakano, "Microstrip-line antennas with loop elements," *IEEE Int. Antennas and Propag. Symp.*, 721–724, 2007.
11. Mittleman, D. and K. Wang, "A method for coupling Terahertz pulses into a coaxial waveguide," Int. Patent, WO 2006/019776 A2, 2008.
12. Jung, C. W., M.-J. Lee, G. P. Li, and F. de Flaviis, "Reconfigurable scan-beam single-arm spiral antenna integrated with RF-MEMS switches," *IEEE Trans. Antennas Propag.*, Vol. 54, No. 2, 455–463, 2006.
13. Balanis, C. A., *Antenna Theory, Analysis and Design*, 2nd Edition, Ch. 4, John Wiley & Sons, New York, 1997.
14. Massaro, A., I. Ingrassio, C. Giordano, M. T. Todaro, R. Cingolani, M. de Vittorio, and A. Passaseo, "Micromachining Mo/AlN/Mo piezoelectric ring resonators," *Proc. of EuMA 2009*, 1646–1649, 2009.
15. Jung, C. W., M.-J. Lee, G. P. Li, and F. de Flaviis, "Reconfigurable scan-beam single-arm spiral antenna integrated with RF-MEMS switches," *IEEE Trans. Antennas Propag.*, Vol. 54, No. 2, 455–463, 2006.